High-pressure structure of half-metallic CrO_2

B. R. Maddox
University of California, Davis, California 95616, USA
and Lawrence Livermore National Laboratory, Livermore, California 94551, USA

C. S. Yoo
Lawrence Livermore National Laboratory, Livermore, California 94551, USA

Deepa Kasinathan, W. E. Pickett, and R. T. Scalettar
University of California, Davis, California 95616, USA

(Received 20 September 2005; revised manuscript received 9 February 2006; published 19 April 2006)

Evidence for a structural phase transition from rutile α-CrO_2 phase I ($P4_2/mnm$) to orthorhombic β-CrO_2 phase II ($CaCl_2$-like, *Pnnm*) is presented using angle-resolved synchrotron x-ray diffraction and high-sensitivity confocal Raman spectroscopy. The transition to the $CaCl_2$ structure, which appears to be second order, occurs at 12 ± 3 GPa without any measurable discontinuity in volume, but is accompanied by an apparent *increase* in compressibility. Raman data are also presented to show further evidence for a second-order structural phase transition as well to demonstrate soft-mode behavior of the B_{1g} phonon mode.

DOI: 10.1103/PhysRevB.73.144111 PACS number(s): 61.10.Nz, 62.50.+p, 64.30.+t, 64.70.Kb

I. INTRODUCTION

Chromium dioxide (CrO_2) has many properties of interest to both the scientific community and industry. It was first introduced as a magnetic recording media in 1974 mainly due to its relatively high coercivity, but has received much more recent attention for its unique electronic properties. First suggested to be half-metallic by Schwarz,[1] CrO_2 has been studied extensively both theoretically and experimentally and has been shown to possess near 100% spin polarization at the Fermi level using superconducting point-contact tunneling experiments.[2] Its half-metallic behavior gives rise to relatively low electrical resistivity for an oxide, $\sim 300\ \mu\Omega$ cm (Ref. 3), and is commonly referred to as a "bad metal." CrO_2 is also ferromagnetic at room temperature with a high Curie temperature of $T_c=390$ K relative to other candidate half-metals. These two properties, along with its already wide availability, make CrO_2 scientifically and technologically important and an ideal material for developing spintronic devices.

CrO_2 is also one of the simplest known half-metals and crystallizes into the rutile structure at ambient conditions, a structure commonly found in many metal dioxides (MO_2; M=Ti, Cr, Mn, Sn, Ge, Pb, etc.). The rutile structure consists of tetragonally distorted edge-sharing MO_6 octahedra (see Fig. 1), one of the most fundamental building blocks of covalently bonded network structures found in hard materials and earth minerals like stishovite. Larger metal ions (i.e., M=W, Re, Mo, etc.), however, tend to form an eightfold-coordinated calcite (CaF_2) structure, while smaller ions (M=C, Si, etc.) crystallize into a fourfold-coordinated tetrahedral structure. At high pressures, the rutile structure typically transforms to another sixfold-coordinated structure, $CaCl_2$, or the α-PbO_2 structure found in shock compressed SiO_2.[4] The smaller fourfold-coordinated SiO_2 transforms into the sixfold rutile structure, stishovite. Therefore, to the first approximation these pressure-induced structural transitions may be understood in the simple view of topological packing of hard spheres, i.e., an increase in the coordination number and the associated electrostatic interaction at high densities.

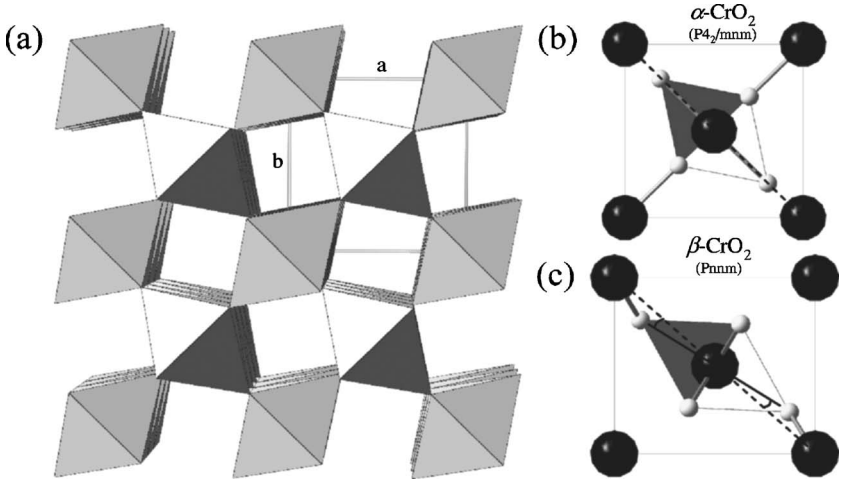

FIG. 1. (a) The edge-sharing octahedra of the rutile structure along the c axis. (b) Shows rutile-structured α-CrO_2 ($P4_2/mnm$, $Z=2$, $a=b=4.421$ Å, $c=2.916$ Å, $u=0.301$) at ambient conditions projected onto the ab plane with Cr^{+4} ions in black and O^{-2} ions in white. (c) Shows β-CrO_2 (*Pnnm*, $Z=2$, $a=4.425$, $b=3.987$, and $c=2.683$, and $u_x=0.371$ and $u_y=0.263$) at 50.4 GPa. The transition from α-CrO_2 to β-CrO_2 involves an orthorhombic distortion and a rotation of the CrO_6 octahedra about the c axis.

At high pressures, however, the electronic structure also changes in a significant way and so does the nature of electron interaction, becoming more repulsive and dominated by electron kinetic energy. As a result, the characteristics of MO_2 transitions could be more complex than is evident from their continuous manner, i.e., occurring without any structural or volume discontinuity. The rutile structure has even been found in the molecular solid CO_2-II at high pressures and temperatures.[5] Furthermore, the electronic contribution to structural stability is significant in transition metal oxides at high pressures, as is evident from the Mott insulator-metal transitions,[6,7] charge transfer transitions,[8] valence transitions, etc.

In the present work, we present a high-pressure structural study of CrO_2 using synchrotron x-ray diffraction and Raman spectroscopy. Evidence for a second-order structural transition at 12 ± 3 GPa from rutile α-CrO_2 phase I to orthorhombic β-CrO2 phase II, accompanied by an increase in compressibility, is presented as well as evidence for soft-mode behavior in the Raman spectrum. A second phase transition is also suggested from anomalies in the x-ray and Raman data around 30 GPa. Finally, the transition pressure for CrO_2 is investigated in the context of other known rutile-$CaCl_2$ transitions at high pressure.

II. EXPERIMENTAL PROCEDURES

Powdered α-CrO_2 was obtained commercially under the name Magtrieve from DuPONT and loaded into Livermore-designed diamond-anvil cells (DACs) in order to achieve pressures up to 50 GPa. Two samples were prepared for x-ray diffraction experiments. One sample was loaded into a 130 μm hole in a Re gasket attached to the piston anvil of a membrane-type cell. Mineral oil was used as a pressure transmitting medium and Au powder was added for pressure determination. The other sample was loaded into the 160 μm hole of a Re gasket attached to the piston anvil of an *LLL* cell along with several small ruby chips for pressure determination using the ruby fluorescence method.[35] The cell was then placed into a Janis Research continuous-flow He cryostat modified for He loading into the *LLL* cell. Liquid He was allowed to accumulate well above the top of the cell, and then the pressure was reduced in the cryostat until superfluid He was obtained. The cell was then opened briefly to allow a small amount of liquid He to leak in and then sealed. A larger sample hole was used, as well as a thicker indentation, to allow for a $\sim$30% volume compression of the liquid He upon loading.

Angle-dispersive x-ray diffraction (ADXRD) data was performed at beamline 16ID-B, HP-CAT at the APS at Argonne National Laboratory using $\lambda=0.3680$ Å x-rays. The synchrotron x-ray beam was focused down to 12×12 μm using a pair of long (0.5 m) Kirkpatrick-Baez bimorph x-ray mirrors, and the partial Debye-Scherrer rings were collected on a Mar345 image plate. Raw x-ray diffraction data were integrated with FIT2D (Ref. 9) and analyzed using XRDA and GSAS. Le Bail whole-profile fitting was used to obtain lattice parameters and profile coefficients, and then a Rietveld refinement was performed to obtain internal oxygen coordinates. Background removal was done manually due to a very irregular amorphous background that was difficult to fit.

For Raman measurements, powdered CrO_2, along with several small ruby chips for pressure determination, was loaded into the 140 μm hole drilled in a Re gasket attached to the piston anvil of an *LLL*-type cell. The cell was then lightly closed and immersed in liquid argon. After the cell came into thermal equilibrium with the surrounding Ar liquid it was then opened briefly to capture a small quantity of argon for use as the pressure transmitting medium. Mineral oil was not used due to the broad, amorphous background generated during previous Raman attempts. Helium was also not used due to the high initial loading pressures required to ensure liquid He capture.

Raman spectra were obtained using a confocal micro-Raman system designed for maximum light collection. A single-stage spectrometer was used for spectra collection along with a pair of Kaiser Supernotch holographic filters for rejection of the Rayleigh scattered light. The 532 nm second harmonic of a diode pumped $Nd:VO_4$ laser was used for Raman excitation. The spot size at the sample was <10 μm. During previous Raman attempts with a conventional Raman setup, sample heating due to the high (100–200 mW) laser powers required would cause a change in oxidation from CrO_2 to Cr_2O_3.[10] These high laser powers were required because the black color and half-metallic nature of the material made the Raman scattered signal very weak. A lower laser power can be used in such a system; however, the long collection times would reduce the density of data points and increase the error in pressure measurement as some cell relaxation occurs during the course of a measurement. A system with high sensitivity was needed to reduce incident laser power to <30 mW while keeping the collection time down to 5 min.

A. X-ray diffraction

At ambient conditions α-CrO_2 crystallizes into the rutile structure ($P4_2/mnm$, $Z=2$) with lattice parameters $a=b=4.421$ Å, and $c=2.916$ Å, and atomic position of Cr($2a$) at (0,0,0) and O($4f$) at $(u,u,0)$ with $u=0.301$.[11] The rutile structure, shown in Figs. 1(a) and 1(b) consists of chains of distorted edge-sharing CrO_6 octahedra along the c axis with the Cr ions forming a body-centered tetragonal lattice. This distortion can work to either flatten (apical bonds are shorter than the equatorial bonds) or elongate (apical bonds are longer than the equatorial bonds) the CrO_6 octahedra along their axes. The positions of the oxygen atoms are determined by the fractional coordinate, u, which sets the Cr-O distances and determines the size and nature of the distortion. Figure 2(a) shows a Rietveld refinement of α-CrO_2 performed at 7.7 GPa, showing a good agreement with the rutile structure with lattice parameters $a=b=4.3710(1)$ Å and $c=2.8967(1)$ Å, and $u=0.294(1)$. At this value of u the CrO_6 octahedra is flattened along the apical direction with Cr-O distances of 1.809 and 1.928 Å for the apical (2) and equatorial (4) bonds, respectively.

At 12.8 GPa an orthorhombic distortion was detected by the splitting of (hkl) diffraction lines with $h\neq k$ as shown in

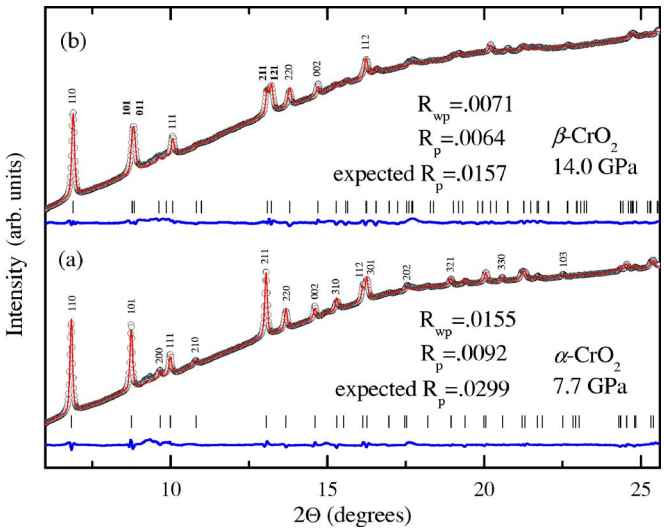

FIG. 2. (Color online) Rietveld refinement of CrO_2 x-ray diffraction data taken at 7.7 and 14.0 GPa. Open circles show experimental data, while red and blue lines show calculated spectra and difference spectra, respectively. Short vertical lines show positions of diffraction lines. (a) shows the structural refinement of rutile α-CrO_2, space group $P4_2/mnm$, while (b) shows the structural refinement of orthorhombic β-CrO_2 in the $CaCl_2$ structure, space group *Pnnm*. Only the strongest (*hkl*)'s are labeled. (*hkl*)'s shown in bold represent those diffraction lines with $h \neq k$ which were split during the orthorhombic distortion from tetragonal $P4_2/mnm$ to orthorhombic *Pnnm*. The values R_{wp}, R_p, and expected R_{wp} were calculated without contributions from the background fit.

Fig. 1(b), with the split (*hkl*)'s shown in bold. This is consistent with the structural transition from rutile to $CaCl_2$ (*Pnnm*, $Z=2$) crystal structures observed in other rutile-type oxides such as MnO_2 (Ref. 12), RuO_2 (Ref. 13), SiO_2 (Ref. 14), GeO_2 (Refs. 15 and 16), SnO_2 (Refs. 17 and 18), and PbO_2 (Ref. 19). The $CaCl_2$ crystal structure consists of chains of distorted edge-sharing CrO_6 octahedra along the *c* axis with the Cr ions forming a body-centered orthorhombic lattice and is shown in Fig. 1(c). The position of the oxygen atom is now described by two fractional coordinates u_x and u_y. The Reitveld refinement [Fig. 2(b)] of β-CrO_2 at 14.0 GPa shows good agreement with the $CaCl_2$ structure with lattice parameters $a=4.3874(4)$ Å, $b=4.2818(4)$ Å, and $c=2.8779(2)$ Å, and $u_x=0.299(1)$ and $u_y=0.272(1)$.

Figure 3 shows lattice constants obtained using a Le Bail whole-profile fit as a function of pressure with a dotted vertical line showing the transition pressure. The diffraction data from the mineral oil sample suffered from broadening of diffraction lines above 9 GPa, due to nonhydrostatic conditions inside the sample chamber,[20] and made refinement difficult to converge. Therefore, we only present data below 9 GPa for this sample as shown in Fig. 3. On the other hand, the diffraction data obtained using He as a pressure medium stayed well resolved up to the highest pressure obtained. Below the transition pressure the compressibility of the *a* axis using mineral oil and He is very close, with the He sample showing a slightly higher compressibility. The *c* axis, however, shows a much lower compressibility when using He as a pressure medium, although it is clear that both curves ex-

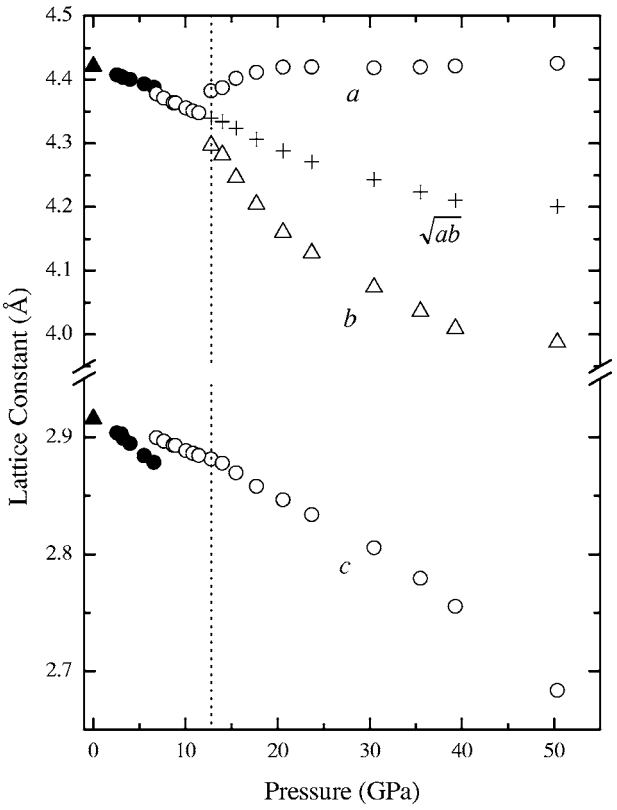

FIG. 3. Lattice constants of CrO_2 as a function of pressure. Open and closed circles represent data taken with helium and mineral oil as a pressure medium. Dark triangles are data obtained by Cloud *et al.* (Ref. 11). Crosses represent the area conserving quantity $\sqrt{ab}$. Vertical dotted line at 12 GPa shows transition from rutile α-CrO_2 to orthorhombic β-CrO_2.

trapolate back to the previously reported value at $P=0$. A change in compressibility at 12.8 GPa is observed for the *c* axis, while the area conserving quantity $\sqrt{ab}$ follows smoothly from the *a* axis across the transition. There is also a small but apparent change in compressibility of the *c* axis at ~25–30 GPa. This change may be a signature of a second phase transition. Additional evidence supporting a second phase transition was observed in our Raman data in this pressure range and is discussed below.

The pressure vs volume data of α- and β-CrO_2 phases are plotted up to 50 GPa in Fig. 4, identifying the transition pressure $P_c=12.8\pm3$. Below P_c the mineral oil and He data agree well, resulting in a nearly identical *P-V* curve. Above P_c an anomalous increase in the compressibility occurs. This is in contrast to most materials becoming stiffer with pressure. The experimental *PV* curve for α-CrO_2 was fit to the third-order Birch-Murnaghan[21] equation of state

$$P=\frac{3}{2}B_0\left[\left(\frac{V}{V_0}\right)^{-7/3}-\left(\frac{V}{V_0}\right)^{-5/3}\right]\left\{1+\frac{3}{4}(B_0'-4)\times\left[\left(\frac{V}{V_0}\right)^{-2/3}-1\right]\right\}, \quad (1)$$

with $B_0'=(dB/dP)_{T;P=0}=4$ and V_0 fixed at the previously reported value of 56.99 Å^3 (Ref. 11) which yielded a value

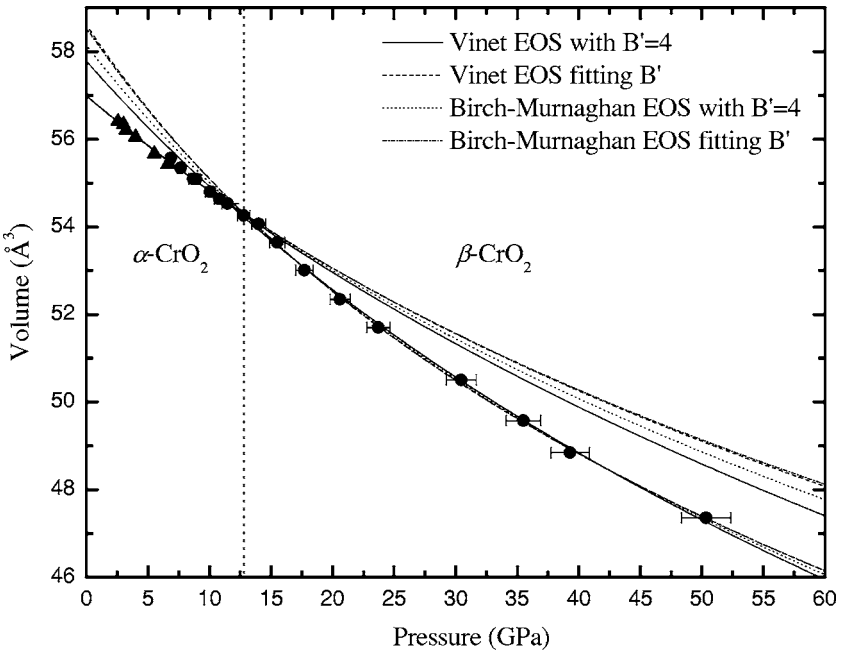

FIG. 4. Pressure vs volume data for CrO_2. Dark circles are data collected using a He pressure medium and dark triangles were collected using mineral oil as the pressure medium. Dotted vertical line denotes transition from rutile α-CrO_2 to orthorhombic β-CrO_2 at 12 ± 3 GPa. Error bars are shown when uncertainties exceed symbol width. Various fits are shown using the Vinet and Birch-Murnaghan equations of state, both with and without fixing $B_0{}'=4$. The numerical results are summarized in Table I.

of $B_0=239\pm2$ GPa for the zero-pressure bulk modulus. The high-pressure β-CrO_2 phase was also fit to Eq. (1) yielding values of $B_0=162\pm2$ GPa and $V_0=58.1\pm.1$ Å^3 for the zero-pressure bulk modulus and unit cell volume, respectively. In addition, we performed Birch-Murnaghan equation of state fits for both phases while letting $B_0{}'$ vary, as well as fits to the Vinet equation of state. These are shown in Fig. 4 and the numerical results of the various fits are summarized in Table I. The fits to the low-pressure phase all give quite similar answers; however, the differences between the various equations of state are evident in the high pressure phase. This is primarily due to the lack of data to constrain V_0 as β-CrO_2 does not exist at ambient conditions. It is clear, however, that a pronounced softening is evident irrespective of the model used to fit the compression data.

B. Raman

The Raman signal of half-metallic CrO_2 is very weak due to the metallic nature of the material which, due to a short penetration depth, results in a relatively small scattering volume and low number of scattering sites.[22] Nevertheless, by using a fast confocal Raman spectroscopy system we were able to obtain relatively high-quality Raman spectra from powdered CrO_2, as shown in Fig. 5, using no more than 30 mW of laser power as measured at the sample. Small features in the Raman spectra below 200 cm^{-1} are, however, obscured because of the use of two holographic notch filters used to prevent Rayleigh scattered light from entering the spectrometer, the result of which was both the introduction of some small spurious peaks and much reduced transmission below 200 cm^{-1}.

A factor group analysis gives four Raman-active modes in the rutile structure, $\Gamma_{Raman}=E_g+A_{1g}+B_{1g}+B_{2g}$. Previous work by Iliev *et al.*[22] using polarized Raman spectroscopy on single-crystal CrO_2 at ambient pressure describes these modes and determined the Raman shifts to be 149, 458, 570, and 682 cm^{-1} for the B_{1g}, E_g, A_{1g}, and B_{2g} modes, respectively. Figure 5 shows our Raman spectra of CrO_2 taken at various pressures. The three peaks at 470, 584, and 700 cm^{-1} shown at 2.8 GPa are associated with the E_g, A_{1g}, and B_{2g} modes of the rutile structure, respectively. Unfortunately, we were not able to observe the Raman-active B_{1g} shear mode, which has been shown to exhibit soft-mode behavior at high pressure in other rutile-$CaCl_2$ (Refs. 14 and 18) transitions, due to its very weak scattering around 150 cm^{-1}.[13]

The expected mode behavior for a phase transition from rutile to $CaCl_2$ is a splitting of the doubly degenerate E_g mode along with the addition of a new Raman active mode

TABLE I. Summary of numerical results from various equation of state fits to our experimental PV data. Numbers shown without error denote values that were fixed during the fitting procedure.

	Birch-Murnaghan			Vinet		
Phase	B_0 (GPa)	$B_0{}'$	V_0 (A^3)	B_0 (GPa)	$B_0{}'$	V_0 (A^3)
I	239±2	4.0	56.99	242±2	4.0	56.99
I	235±10	5±2	56.99	235±10	6±2	56.99
II	162±2	4.0	58.1±0.1	181±3	4.0	57.8±0.1
II	143±16	4.8±0.7	58.5±0.4	138±16	5.8±0.7	58.6±0.4

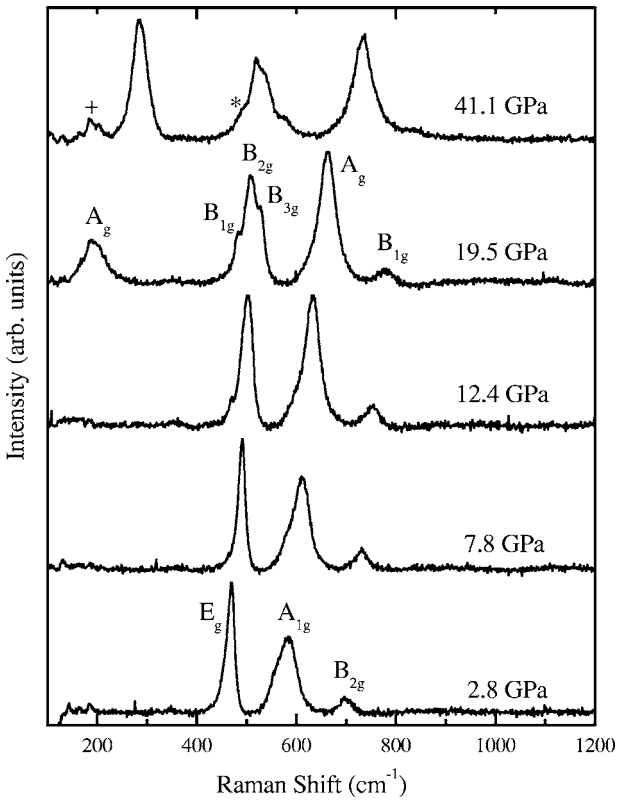

FIG. 5. Raman spectra of CrO_2 at 532 nm excitation at various pressures. At 12.4 GPa the broadening of the E_g mode due to a splitting and the appearance of a new mode at 470 cm^{-1} are consistent with a phase transition from rutile to $CaCl_2$ structures. We also see the appearance of the Raman-active A_g mode in $CaCl_2$ as shown at 19.5 GPa. The asterisk marks an unidentified peak occurring at 32 GPa and persisting up to the highest pressure obtained during this experiment. A broad background has been subtracted from all spectra. The cross marks an intermittent peak caused by a combination of the holographic notch filters and the background subtraction and does not shift consistently with pressure.

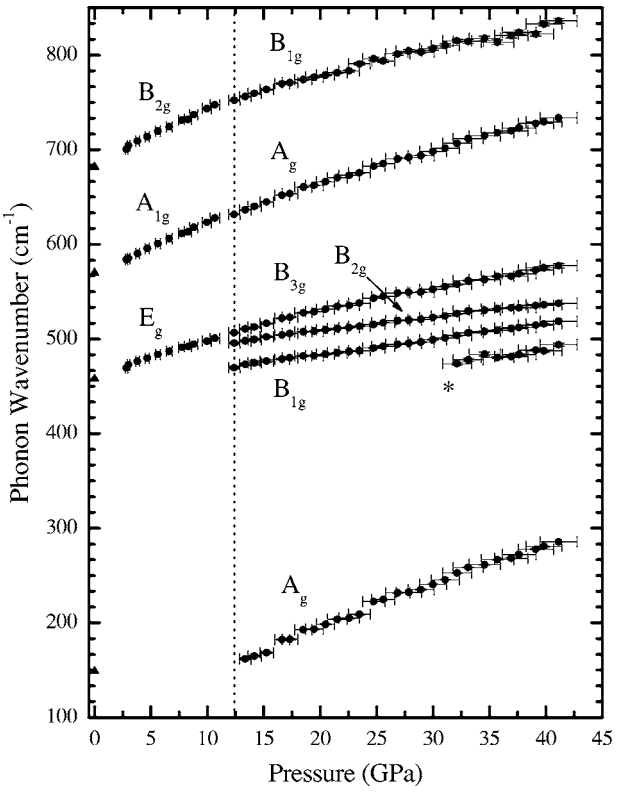

FIG. 6. Plot of CrO_2 phonons vs pressure in the rutile and $CaCl_2$ structures. Dark triangles show ambient pressure values obtained by Iliev *et al.* (Ref. 22) on single-crystal CrO_2. Dark circles represent our data. Dotted vertical line at 12 GPa denotes the transition from tetragonal α-CrO_2 to orthorhombic β-CrO_2 derived from our experimental data.

of B_{1g} symmetry.[13] At 12.4 GPa a new peak appears at 470 cm^{-1} and the E_g mode begins to broaden. By 19.5 GPa a clear splitting of the E_g mode is observed along with an additional peak emerging at 162 cm^{-1}. Mode assignments for phase II are based primarily on the correlation between rutile (D_{4h}) and $CaCl_2$ (D_{2h}) modes, except for the new Raman-active mode of B_{1g} symmetry which is tentatively assigned to the new peak at 470 cm^{-1} and assumed to be accidentally degenerate. The order of the B_{2g} and B_{3g} modes shown is arbitrary as it has been argued that the sign of the spontaneous strain, $e_{ss}=(a-b)/(a+b)$, determines the ordering.[23] Because all our experiments were done on powdered samples and not single crystals, the sign of e_{ss} is unknown. It should also be noted that a seventh, unassigned peak was observed at 33 GPa, identified with an asterisk, showing a variation with pressure consistent with the other, identified peaks. The small peak around 185 cm^{-1} at 41.1 GPa, marked with a cross in Fig. 5, was intermittent and did not seem to show any consistent behavior with pressure. This peak is therefore attributed to spurious noise caused by the pair of holographic notch filters coupled with the background subtraction procedure.

Figure 6 shows the pressure-induced shifts of the observed Raman modes for α- and β-CrO_2. Although we were unable to directly observe any mode-softening behavior due to the weakness of the B_{1g} shear mode in rutile α-CrO_2, we can speculate that in order for the B_{1g} mode to smoothly connect to the A_g mode there must have been some softening. Figure 6 shows ambient pressure values obtained from Iliev *et al.*[22] for all four Raman-active modes in rutile CrO_2 as dark triangles. It is clear that a smooth curve can be drawn between the ambient pressure values and our data for the E_g, A_{1g}, and B_{2g} modes, but not for the B_{1g} mode. This is further evidence that β-CrO_2 takes the $CaCl_2$ structure since softening of the B_{1g} mode has been seen in many of the rutile-$CaCl_2$ transitions.[14,18,15] It should again be noted that the unidentified peak showing up at 33 GPa, marked with an asterisk in Fig. 6, shows a pressure-induced shift consistent with the rest of the identified modes.

III. DISCUSSION

The present x-ray data reveal that the rutile-to-$CaCl_2$ transition in CrO_2 is a strain-driven, second-order distortive phase transition. The crystal structures of both phases (see Fig. 1) consist of distorted edge-sharing CrO_6 octahedra where the degree of distortion increases upon moving from α-CrO_2 to β-CrO_2. For example, at ambient conditions the

four equatorial Cr-O bonds in the [110] plane are at 1.917 Å and lie roughly along the *c* axis, while the other two apical Cr-O bonds in the $1\bar{1}0$ plane are at 1.882 Å and lie parallel to the *ab* plane. At the onset of the transition at 12.4±3 GPa the disparity in Cr-O distances increases to 1.930 Å for the equatorial bond and 1.795 Å for the apical bond. This local strain arising from the large disparity in bond lengths along the *c* axis and *ab* plane results in a large compressibility along the *c* axis with respect to the *a*- and *b* axes (see Fig. 3) and an increase of the O-O contact distance to 2.568 Å for β-CrO_2 from the relatively short 2.488 Å in α-CrO_2. This short O-O distance in α-CrO_2 may induce the softening of the B_{1g} mode inferred from the present Raman data, shown in Fig. 6, and cause a mechanical instability of the rutile structure.[24,25]

It is often difficult to correctly determine the order of a phase transition through structural measurements alone. Recall that the splitting of the (101) diffraction peak into (101) and (011) peaks is seen clearly at 12.8 GPa. However, broadening of the (101) peak before 12.8 GPa was also detected, which could indicate a continuous second-order transition that begins before 12.8 GPa. This is illustrated in Fig. 3, where a discontinuity in the lattice parameters is shown at 12.8 GPa; however, extrapolation of the *a*- and *b*-axis curves from β-CrO_2 back to the *a* axis from α-CrO_2 could indicate a continuous transition beginning as low as 10.8 GPa. Indeed, in many other rutile-type oxides[13,17,12] the transition to the $CaCl_2$ structure has been shown to be second order with the spontaneous strain, $e_{ss}=(a-b)/(a+b)$, as the order parameter. According to Landau's theory of second-order phase transitions, the order parameter should be proportional to $(P-P_c)^{1/2}$. To examine this possibility, we have plotted e_{ss}^2 vs pressure in Fig. 7(a). Our data appear very linear up to 25 GPa with a fit to a straight line giving a value of P_c

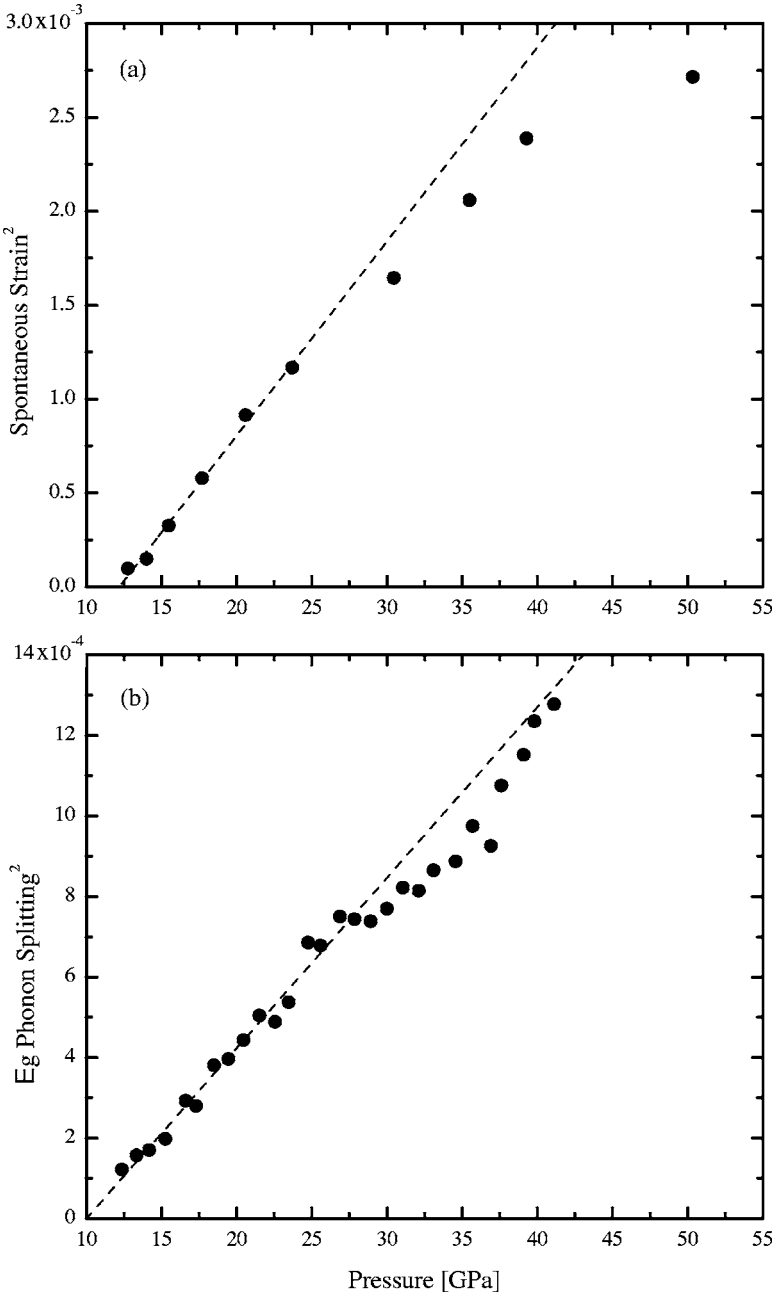

FIG. 7. Plot of the square of the (a) spontaneous strain, defined as $(a-b)/(a+b)$, and (b) E_g phonon splitting, defined as $(\nu_1-\nu_2)/(\nu_1+\nu_2)$, vs pressure. Dotted lines show a linear fit of the form $A^2(P-P_c)$ up to 25 GPa giving $P_c=10.00$ GPa for (a) and $P_c=12.20$ GPa for (b). Deviations from linearity are clear above 25 GPa.

=12.2 GPa. Above 25 GPa, however, strong deviations from linearity are observed. The splitting of the E_g mode in rutile materials has been shown to be directly proportional to the spontaneous strain and should therefore also follow a $(P-P_c)^{1/2}$ scaling.[26] The square of this splitting is plotted in Fig. 7(b). We again see good linearity up to 25 GPa, giving a value of $P_c=10.0$ GPa, above which we see deviations. The agreement with $(P-P_c)^{1/2}$ below 25 GPa suggests that this is indeed a second-order transition. Although this scaling only rigorously applies near the transition pressure, the deviations at 25 GPa coincide with the new Raman peak observed at 33 GPa and the change in compressibility of the *c* axis, and could indicate the appearance of a new phase. However, no indication of a second structural phase transition was found in the x-ray diffraction data. Therefore, further experiments are needed to make a solid conclusion.

The lower value of P_c obtained from our Raman data, compared to x ray, is likely due to the use of different pressure media: argon for Raman and He for x-ray diffraction. Argon is known to provide slightly less hydrostatic conditions than He and therefore could have forced the transition to occur at a lower pressure during the Raman experiment. In addition, the larger compressibility of the *c* axis observed in α-CrO_2 using mineral oil compared to that obtained using He, shown in Fig. 2, is also suggestive of a greater strain than in He. It has been shown by Haines *et al.*[17] that the rutile$\rightarrow$$CaCl_2$ transition is very sensitive to nonhydrostatic stress, and the use of nonhydrostatic pressure media can lower the transition pressure by as much as 8 GPa for SnO_2. Therefore, we place the transition at 12 ± 3 GPa based on the first appearance of a clear splitting of the diffraction lines with $h\neq k$ and estimate the experimental uncertainty to be $\sim$3 GPa due to the discrepancy in P_c discussed above.

It is interesting to note that extrapolated zero-pressure bulk modulus of β-CrO_2 is lower than that of α-CrO_2 going from $B_0=239\pm2$ to $B_0=162\pm2$ GPa across the phase transition (see Fig. 3 and Table I). Lattice softening is not uncommon for strain-driven distortive-type transitions at high pressures, as seen in materials like ReO_3 and UO_3, where the softening occurs as a result of "buckling" of the linear Re–O bonds.[27,28] As previously discussed and shown in Fig. 3, the change in volume compressibility comes largely from an increase in compressibility of the *c* axis, not from a change in compressibility of the *ab* plane as evident from the area conserving parameter $\sqrt{ab}$. A similar lattice softening has also been seen during the high-pressure rutile$\rightarrow$$\alpha$-$PbO_2$ transition in TiO_2 and PbO_2 which also involves a large change in the compressibility of the *c* axis.[19,29] In these materials the change in compressibility is due to the way the O-octahedra link along the *c* axis, forming zigzag edge-sharing chains instead of straight edge-sharing chains as in rutile. This increases the number of distortion mechanisms and results in a larger compressibility. The rutile-$CaCl_2$ transition, however, does not alter the way O-octahedra link along the *c* axis and may therefore need an alternative explanation for the lattice softening.

The tetragonal distortion (apical Cr-O bond is shorter than the equatorial bonds) of the CrO_6 octahedra introduced in α-CrO_2 splits the doubly degenerate e_g molecular orbital into a_{1g} and b_{2g} states and splits the triply degenerate t_{2g} orbital into b_{2g} and e_g.[30] The orthorhombic distortion in β-CrO_2 further splits this latter e_g orbital into b_{2g} and b_{3g} orbitals. As a result, the two unpaired *d* electrons in d^2 CrO_2 can be paired up in the lowest energy *d* orbital, either b_{2g} or b_{3g}, in a sufficiently strong crystal field. This would be equivalent to removing the exchange splitting of the up-spin and down-spin *d* states and increasing the metallic character of CrO_2. Lattice softening due to changes in the electronic structure has been seen in a variety of materials. In the monochalcogenides of the rare earths, such as TmTe, the anomalous increase in compressibility with pressure is attributed to continuous $4f$-$5d$ electron promotion, resulting in a semiconductor-metal transition.[31] Shock experiments on liquid D_2 indicate a significant increase in compressibility accompanying the insulator-metal transition.[32] We therefore postulate that the increase in compressibility of CrO_2 at 12 GPa may be due to an electronic transition from half-metal to metal. Recent electronic structure calculations support this conjecture by showing that the density of state is much more sensitive to changes in the *c* axis than either the *a*- or *b* axis.

TABLE II. Rutile to $CaCl_2$ transformation pressures and ambient pressure anion radii, degree of MO_6 distortion, and B_{1g} mode frequencies for various metal oxides.

MO_2 compound	Transition pressure (GPa)	Anion radii[a] (Å)	MO_6[b]	B_{1g} frequency (cm^{-1})
TiO_2[c]	7	0.745	0.008	141
CrO_2	12.2	0.69	0.009 16	149
MnO_2	0.3	0.68	0.003 45	
RuO_2	11.8	0.76	0.011 26	165
SiO_2	50	0.54	0.014 5	232
GeO_2	26.72	0.68	0.009 01	171
SnO_2	11.8	0.83	0.002 48	158
PbO_2	4	0.915	0.003 09	

[a]Anion radii obtained from Ref. 34 for the 4th oxidation state and 6-fold coordination.
[b]Structural information for metal oxides at ambient conditions is summarized in Ref. 33.
[c]Transition pressure for rutile to α-PbO_2 in TiO_2.

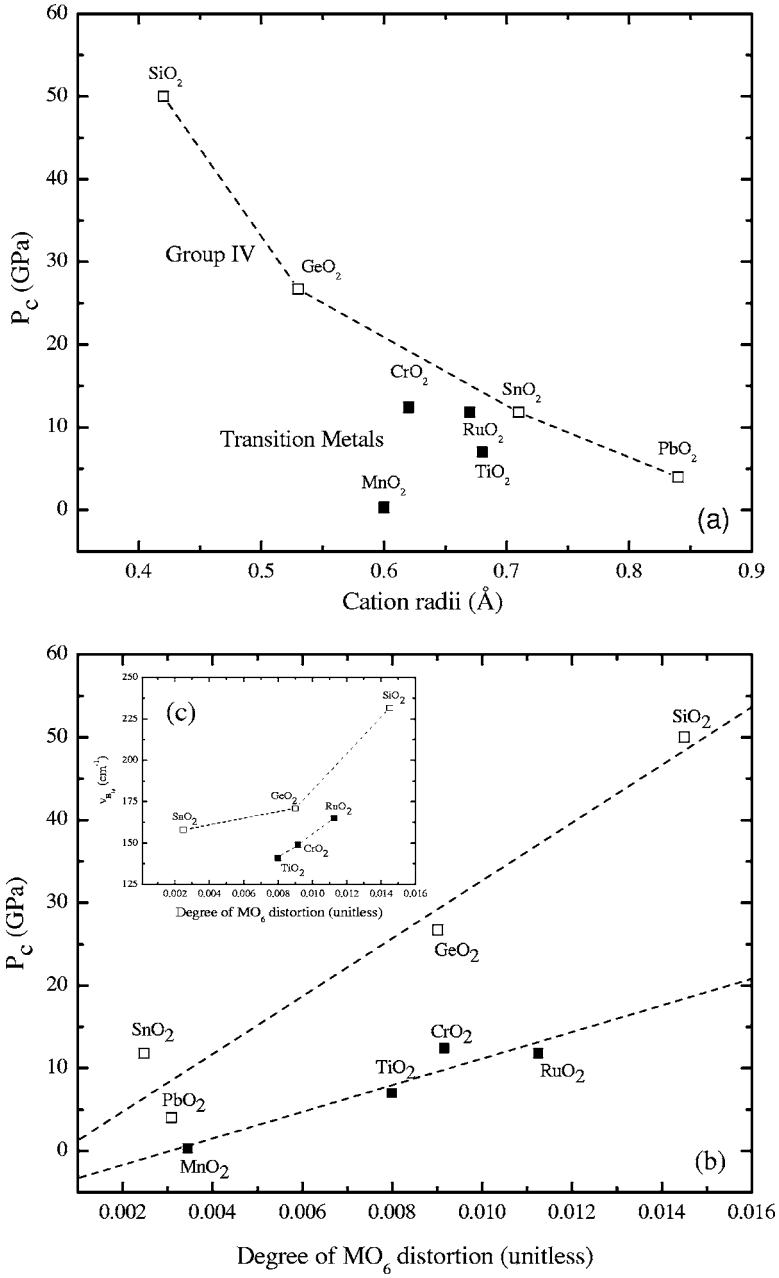

FIG. 8. (a) Metallic ion radii for select MO_6 compounds vs transition pressure, P_c. Open squares show group-IV oxides and dark squares show transition-metal oxides. Dotted line serves as a guide to the eye to show the trend of increasing transition pressure with decreasing anion radii. (b) shows plot of the ambient pressure MO_6 distortion, defined as $|(a-b)/(a+b)|$ where $a \equiv$ apical M-O distance and $a \equiv$ equatorial M-O distance, vs transition pressure (left axis, squares) and B_{1g} mode frequency (right axis, triangles). Light and dark squares represent the group-IV and transition metal oxides, respectively. Dashed lines are linear fits showing increasing transition pressure with increasing MO_6 distortion. Inset (c) shows increase of B_{1g} mode frequency with increasing distortion.

The transition observed in the present study is in accordance with other MO_2-type transition metal or group-IV dioxides taking the rutile structure. For example, rutile-type MnO_2 undergoes a phase transition at 0.3 GPa to the $CaCl_2$ structure and possibly another phase transition around 46 GPa to an unknown cubic phase.[12] Other materials often undergo postrutile phase transition to structures such as α-PbO_2, α-cristobalite, etc. Table II summarizes the results for many MO_2 compounds. To compare CrO_2 with the rutile-type compounds at high pressure and to gain insight into the systematics of these transitions, we have plotted the metallic ion radii vs transition pressure in Fig. 8(a). It should be noted that the structural results from Table II were taken from Bolzan *et al.*;[33] however, the values for the ionic radii were taken from Shannon and Prewitt.[34] The values used in Ref. 33 are those obtained by Ahrens which do not account for coordination number and spin state and, consequently, do not give the correct values for the anion-cation distances when added together. We see strong systematics in the group-IV metal dioxides showing increasing transition pressure with decreasing anion radius. The transition metals, however, show much more complex behavior.

To elucidate the connection between transition pressure and ambient pressure crystal structure parameters, we have also calculated the degree of MO_6 octahedra distortion at ambient pressure, defined as $|(r_1-r_2)/(r_1+r_2)|$, where $r_1 \equiv$ apical M-O distance and $r_2 \equiv$ equatorial M-O distance. The values are plotted as a function of transition pressure in Fig. 8(b). It suggests that a higher degree of distortion leads to a dramatic increase in the stability range of the rutile structure. α-CrO_2, with an ambient pressure value of 0.009 16, agrees well with the other transition-metal com-

pounds. It should also be noted that although the group-IV compounds and transition-metal compounds both follow a nearly linear trend, the line of transition-metal compounds is below that of group IV. We can try to understand this behavior by looking at the B_{1g} vibrational mode frequency, ν_{B1g}, at ambient pressure for the various MO_2 compounds as a function of transition pressure. This is plotted in Fig. 8(c). We can see that an increased distortion of the MO_6 leads to an increase in ν_{B1g}. Since the rutile-$CaCl_2$ transition is driven by a mechanical instability with the same symmetry as the B_{1g} mode, demonstrated by softening of this mode, a material with a higher ambient pressure value for ν_{B1g} may take longer to transform, leading to a higher value for P_c. The fact that for a given degree of distortion the values for ν_{B1g} for the transition-metal oxides are systematically lower, leading to lower values for P_c, may be electronic in nature. The bonding between M-O in the transition metal oxides is dominated by its partially filled d orbitals, where in the group-IV compounds this same bonding has predominantly p character.

ACKNOWLEDGMENTS

We would like to thank the entire High Pressure Physics Group staff at LLNL for their technical and scientific guidance. We also thank HPCAT beamline scientist Maddury Somayazulu for his technical assistance. Use of the HP-CAT facility was supported by DOE-BES, DOE-NNSA (CDAC), NSF, DOD-TACOM, and the W. M. Keck Foundation. Use of the Advanced Photon Source was supported by the U. S. Department of Energy, Office of Science, Office of Basic Energy Sciences, under Contract No. W-31-109-Eng-38. This work has been supported by the SEGRF and LDRD programs at LLNL, University of California, U. S. DOE No. W-7405-ENG-48, and by the SSAAP at UCD, DOE DE-FG03-03NA00071.

[1] K. Schwarz, J. Phys. F: Met. Phys. **16**, L211 (1986).
[2] Y. Ji, G. J. Strijkers, F. Y. Yang, C. L. Chien, J. M. Byers, A. Anguelouch, Gang Xiao, and A. Gupta, Phys. Rev. Lett. **86**, 5585 (2001).
[3] Katsihiko Suzuki and P. M. Tedrow, Phys. Rev. B **58**, 11597 (1998).
[4] T. G. Sharp, A. El Goresy, B. Wopenka, and M. Chen, Science **284**, 1511 (1999).
[5] C. S. Yoo, H. Kohlmann, H. Cynn, M. F. Nicol, V. Iota, and T. LeBihan, Phys. Rev. B **65**, 104103 (2002).
[6] J. R. Patterson, C. M. Aracne, D. D. Jackson, V. Malba, S. T. Weir, P. A. Baker, and Y. K. Vohra, Phys. Rev. B **69**, 220101(R) (2004).
[7] C. S. Yoo, B. Maddox, J.-H. P. Klepeis, V. Iota, W. Evans, A. McMahan, M. Y. Hu, P. Chow, M. Somayazulu, D. Hausermann, R. T. Scalettar, and W. E. Pickett, Phys. Rev. Lett. **94**, 115502 (2005).
[8] A. L. Chen, P. Y. Yu, and R. D. Taylor, Phys. Rev. Lett. **71**, 4011 (1993).
[9] A. P. Hammersley, *ESRF Internal Report* ESRF97HA02T, FIT2D V9.129 Reference Manual V3.1 (1998).
[10] T. Yu, Z. X. Shen, J. He, W. X. Sun, S. H. Tang, and J. Y. Lin, J. Appl. Phys. **93**, 3951 (2003).
[11] W. H. Cloud, D. S. Schreiber, and K. R. Babcock, J. Appl. Phys. **33**, 1193 (1962).
[12] J. Haines, J. M. Leger, and S. Hoyau, J. Phys. Chem. Solids **56**, 965 (1995).
[13] S. S. Rosenblum, W. H. Weber, and B. L. Chamberland, Phys. Rev. B **56**, 529 (1997).
[14] K. J. Kingma, R. E. Cohen, R. J. Hemley, and Ho-kwang Mao, Nature (London) **374**, 243 (1995).
[15] J. Haines, J. M. Leger, C. Chateau, R. Bini, and L. Ulivi, Phys. Rev. B **58**, R2909 (1998).
[16] Shigeaki Ono, Kei Hirose, Norimasa Nishiyama, and Maiko Isshiki, Am. Mineral. **87**, 99 (2002).
[17] J. Haines and J. M. Leger, Phys. Rev. B **55**, 11144 (1997).
[18] Holger Hellwig, Alexander F. Goncharov, Eugene Gregoryanz, Ho-kwang Mao, and Russel J. Hemley, Phys. Rev. B **67**, 174110 (2003).
[19] J. Haines, J. M. Leger, and O. Schulte, J. Phys.: Condens. Matter **8**, 1631 (1996).
[20] U. Ponkratz, F. Porsch, G. Wortmann, and W. B. Holzapfel, J. Alloys Compd. **359**, 99 (2003).
[21] F. Birch, J. Appl. Phys. **9**, 279 (1938).
[22] M. N. Iliev, A.P. Litvinchuk, H.-G. Lee, C. W. Chu, A. Barry, and J. M. D. Coey, Phys. Rev. B **60**, 33 (1999).
[23] W. H. Weber, G. W. Graham, and J. R. McBride, Phys. Rev. B **42**, 10969 (1990).
[24] J. F. Mammone and M. Nicol, J. Phys. Chem. Solids **42**, 379 (1981).
[25] C. Lee and X. Gonze, J. Phys.: Condens. Matter **7**, 3693 (1995).
[26] P. Merle, J. Pascual, J. Camassel, and H. Mathieu, Phys. Rev. B **21**, 1617 (1980).
[27] J. E. Schirber and B. Morosin, Phys. Rev. Lett. **42**, 1485 (1979).
[28] T. I. Dyuzheva, N. A. Bendeliani, V. V. Brazhkin, and L. M. Kuznetshov, J. Alloys Compd. **315**, 59 (2001).
[29] J. Haines and J. M. Leger, Physica B **192**, 233 (1993).
[30] S. Sugano, Y. Tanabe, and H. Kamimura, *Multiplets of Transition Metal Ions in Crystals* (Academic Press, New York, 1970), Vol. 34.
[31] A. Chatterjee, A. K. Singh, and A. Jayaraman, Phys. Rev. B **6**, 2285 (1972).
[32] R. Cauble, P. M. Celliers, G. W. Collins, L. B. Da Silva, D. M. Gold, M. E. Foord, K. S. Budil, and R. J. Wallace, Astron. Astrophys., Suppl. Ser. **127**, 267 (2000).
[33] A. Bolzan, C. Fong, B. J. Kennedy, and C. J. Howard, Acta Crystallogr., Sect. B: Struct. Sci. **53**, 373 (1997).
[34] R. D. Shannon and C. T. Prewitt, Acta Crystallogr., Sect. B: Struct. Crystallogr. Cryst. Chem. **25**, 925 (1969).
[35] H. K. Mao, J. Xu, and P. M. Bell, J. Geophys. Res. **91**, 4673 (1986).